RSC Advances

PAPER

View Article Online
View Journal | View Issue

Cite this: *RSC Adv.*, 2024, **14**, 23352

Preparation of a CPVC composite loose nanofiltration membrane based on plant polyphenols for effective dye wastewater treatment

Noor Khatoon,[a] Nadir Ali,[b] Sagar Ali,[c] Zhang Chen,[a] Wang Jun*[a] and Honghai Yang*[d]

The textile industry's high-salinity wastewater presents a significant difficulty for fractioning salts and dyes. To fractionate the dyes and salts, a high-performance CPVC composite loose nanofiltration membrane (LNM) was fabricated by interfacial polymerization. The organic phase was obtained by crosslinking polyethylenimine (PEI) with tannic acid (TA) and gallic acid (GA) using TMC. The resultant composite LNM performance was enhanced by adjusting the coating parameters, which included TA and GA concentrations as well as coating time. The study examined the effects of the total content of TA/PEI and GA/PEI concentrations on the chemical structure, surface roughness, and microstructure of the selective layer of LNM using SEM, AFM, FTIR, and water contact angle measurements. It also investigated the filtration performance of the membrane's selective layer, including pure water flux, PEG800 rejection rate, and membrane fouling analysis. However, the resultant membrane treated simulated reactive black 5 (RB5) dye wastewater. When the total content of TA/PEI is 4 kg L^{-1}, the permeability of pure water flux is high at 7.5 L per m^2 per h per bar when the total content of GA/PEI is 14 kg L^{-1} and the pure water flux is high at 8.8 L per m^2 per h per bar. The overall PEG800 rejection rates were 97–98.98%. The optimal TA : PEI ratios reached a good pure water permeability up to 6.4 L per (m^2 per h per bar) with a high rejection rate of 99.69% for a ratio 1/3 to dye, and GA : PEI ratios reached a good water permeability at 5.5 and 6.5 L per (m^2 per h per bar) with rejection rates of 99.21% and 98.88% for ratio 1/3 and 3.5/10.5 for simulated RB5 dye, and the NaCl retention rate gradually decreased from 4% to 3%. The resultant LNM demonstrated promising applications in dye and salt fractionation.

Received 15th May 2024
Accepted 18th July 2024

DOI: 10.1039/d4ra03570d

rsc.li/rsc-advances

1. Introduction

Concern over the lack of clean water resources is spreading around the world.[1] An estimated 67% of the world's population is predicted to face water stress by 2025.[2] Meanwhile, the excessive release of hazardous dye-containing textile wastewater into the environment has drawn a lot of attention.[3] The effluent from textiles typically comprises sodium sulfate (Na_2SO_4) or sodium chloride (NaCl).[4,5] Conventional techniques like chemical oxidation, absorption, and coagulation often lead to low separation efficiency, resource waste, and secondary pollution.[6] Upgrading is indicated for efficient recovery and cyclic use of high-value-added commodities.[7] Consequently, if this effluent is not handled properly, it will seriously harm both the environment and people.

Membrane technologies have been explored as a viable option for wastewater treatment that is sustainable due to their various benefits, including high separation efficiency, minimal energy use, and flexibility in operations.[8–15] As one of the common membrane technologies, nanofiltration (NF) has been crucial in the removal of heavy metals from wastewater and pharmaceutical reclamation.[16,17] The pore size of NF membranes was typically between 0.5 and 2.0 nm, which made it possible for the membranes to efficiently remove organic materials or multivalent salts with molecular weights between 200 and 1000 Da.[18,19] To separate inorganic salts and organic molecules with less pressure and more flow, loose

[a]College of Environmental Science and Engineering, Donghua University, Shanghai, 201620, China. E-mail: wangj@dhu.edu.cn
[b]Department of Textile Engineering, Mehran University of Engineering & Technology, Jamshoro, 76060, Pakistan
[c]Department of Environmental Engineering, Mehran University of Engineering & Technology, Jamshoro, 76060, Pakistan
[d]Department of Civil Engineering, Donghua University, Shanghai, 201620, China. E-mail: yhh@dhu.edu.cn

nanofiltration membranes (LNMs), a form of pressure-driven membrane, are an alternative to NF developed in 2004, according to Van der Bruggen *et al.*[20–23]

Compared to a typical TFC NF membrane, composite LNMs had a looser skin layer, which allowed for better permeability and effective salt permeation while maintaining a high rejection rate for organic dyes.[16,17,20,24–28] The aforementioned skin layer was attempted to be obtained using interfacial polymerization.[29–31] In order to loosen the skin layer, the focus of these experiments was on developing extended monomers or adding suitable nanofillers. Even though significant advances were made in obtaining better loose nanofiller performance, several innate problems remained. These included the absence of efficient interactions between fillers and the matrix, the agglomeration of nanoparticles, and intricate pre-synthesis protocols for certain monomers.[32] As such, the issue of developing straightforward and trustworthy methods for the preparation of long nanomaterials persists. Numerous LNMs have been described as a result of the advancement of membrane fabrication technology.[33] Polymeric membranes were a common choice among them because of the vast variety of materials with various properties, low cost, and simplicity of manufacture.[34] Plant polyphenol-inspired coatings enhance membrane surface stability and hydrophilicity by forming strong cross-links with membrane surfaces. This creates a dense network of chemical bonds, sealing the surface and enhancing adhesion. The concentration of plant polyphenols also impacts the selective layer of nanofiltration membranes, enhancing their separation capabilities. These compounds work synergistically, enhancing membrane stability and selectivity.

It has been strongly shown that polyphenols are an effective alternative for developing and modifying polymeric membranes.[35–37] Because polyphenols naturally include either pyrogallol or catechol structures, they are useful reagents for surface engineering and functionalization. Tannic acid (TA), an affordable and easily obtainable polyphenol, has demonstrated flexibility in membrane production. TA can be used as a modifier of polymeric membranes,[35,38,39] an addition in the casting solution of non-solvent-induced phase separation (NIPS),[38,40,41] or even as a monomer during the IP procedure.[42] TA can undergo oxidation to TA-quinone in alkaline conditions, subsequently engaging in reactions with amino groups through Michael addition/Schiff base reactions.[22,43] These reactions find extensive applications in functional coating, surface immobilization, and selective layer development in aqueous environments.[15,44–48] These characteristics enable TA to interact with amino monomers such as PIP and polyethyleneimine (PEI), producing products notably longer than those derived from PIP/PEI or TA alone. The extended polymer chains and slow diffusion rates of longer monomers impede the dense packing of the active layer, resulting in a looser active layer and larger pores after polymerization with TMC.[49,50] However, no research has been published on the manufacture of composite CPVC loose nanofiltration membranes as basis materials with TA and GA added to aqueous phase monomers.

This work is inspired by the properties of plant polyphenols such as TA and GA. The study looks into the development and use of a CPVC composite loose nanofiltration membrane infused with plant polyphenols, such as tannic acid (TA) and gallic acid (GA), to treat dye wastewater. By combining CPVC, TA, and GA, the membrane gains improved capabilities for filtering dye molecules while preserving water permeability. This environmentally friendly strategy makes use of natural substances and appears to be a promising solution for tackling environmental issues caused by dye wastewater pollution. The study's findings emphasize the membrane's potential for efficient and sustainable wastewater treatment applications.

2. Materials and methods

2.1 Materials

Donghui Plasticizing Raw Materials Co., LTD. supplied chlorinated polyvinyl chloride (CPVC). *N*,*N*-Dimethylacetamide (DMAc, analytically pure), hydrogen peroxide (H_2O_2, 30%), *n*-hexane (C_6H_{14}, analytically pure), reactive black 5 dye (RB5), sodium chloride (NaCl, superior pure) was supplied by Sinopod Chemical Reagents Co., LTD. Gallic acid (Rowan's reagent); tannic acid, polyethyleneimine (PEI, relative molecular mass 1800), Tris-HCl buffer solution (pH = 8.5), trimesoyl chloride (TMC, 98%), polyethylene glycol (PEG800) was bought from Shanghai McLean Biochemical Technology Co., LTD.

2.2 Instruments and characterization

The MSC cup ultrafilter (300 mL, Motorcycle Science Equipment Co., LTD) is used alongside a conductivity meter (DDS-11A, Shanghai Letchi Company, China). Also, a field emission scanning electron microscope (SEM, Model S-4800, Carl Zeiss, Germany), an atomic force microscope (AFM, Dimension Icon, Bruker, Germany), an Ultraviolet-visible spectrophotometer (UV-vis, UV-7504PC, Shimadzu, Japan), a Fourier infrared spectrometer (FTIR, Nicolet 6700, Thermo Fisher Technology Co., LTD.), a total organic carbon analyzer (TOC-5000A, Manmerbol GMBH, Germany), and a Contact Angle Gauge (Model SL200KS) are utilized for analysis.

2.3 Preparation of composite loose nanofiltration membrane

2.3.1 Preparation of base membrane. A specified quantity of CPVC, F127, and DMAC were combined in a conical bottle, thoroughly mixed, and stirred in a temperature-controlled water bath until achieving a consistent and transparent casting solution. Subsequently, the casting solution was placed over a dry and pristine glass plate and evenly spread with a glass rod at a consistent pace to create a film with a thickness of 0.2 mm. Following this, the film was promptly submerged in a gel bath and removed after phase separation occurred. Lastly, it was rinsed with purified water to eliminate the solvent and stored in deionized water for future utilization.

2.3.2 Preparation of CPVC composite LNF membrane. Dissolve tannic acid and gallic acid in 10 mL of Tris buffer solution (pH = 8.5). Once the mixture has completely dissolved,

add 10 mL of a concentration-defined PEI solution. Once the solution is ready, pour the mixed solution on the CPVC base film, which is fixed in the silicon frame. Co-deposit it for a period of 1 hour. After co-deposition for 1 hour the remaining sedimentation liquid was removed from the film's surface by washing it with deionized water. The membrane was dried at a constant temperature in the oven for one hour at 35 °C. Once the membrane has been completely dried, remove it from the oven. After that, a certain amount of 0.2% TMC *n*-hexane solution was added for 5 minutes, then the membrane was removed and dried in an oven at 50 °C for 15 minutes. Lastly, the membrane is ready for use. The dosage and reaction time of the chemicals are shown in Table 1, and the changes in the membrane during the experiment are shown in Fig. 1.

2.4 Characterization of CPVC composite loose nanofiltration membrane

Attenuated total reflection Fourier transform infrared spectrometer (ATR-FTIR) was used to analyze the chemical structure of the nanofiltration membrane and the functional groups of selective layers of the loose nanofiltration membrane. The surface and cross-sectional morphologies of the CPVC composite loose nanofiltration membrane were examined using scanning electron microscopy (SEM, Model S-4800). Furthermore, the atomic force microscope (AFM) was used to determine the surface microstructure and morphology of the samples.

2.5 Hydrophilicity test of composite loose nanofiltration membrane

The hydrophilicity of the composite nanofiltration membrane was measured through a contact angle meter using the static droplet method, and the measurement results were recorded by Young–Laplace fitting. The hydrophilicity of the membrane is determined by measuring its water contact angle. The surface of the nanofiltration membrane is hydrophilic if the contact angle is less than 90° and hydrophobic if it is larger than 90°.

2.6 Filtration performance test of CPVC composite LNF membrane

The performance of the membrane was evaluated on a pure water flux test and a molecular weight cut-off test. With an effective permeable area of 36.6×10^{-4} m^2, the nanofiltration membrane was fixed in the ultrafiltration cup (MSC cup type) after being trimmed to the proper size. First, the membrane was pre-pressurized for 60 minutes at a pressure of 0.15 MPa using deionized water. Subsequently, the nanofiltration membrane's pure water flux was assessed at a pressure of 0.1 MPa, and the filtrate volume was recorded for one hour. Eqn (1) provides the calculation of the pure water flux.

$$J_w = \frac{V}{At} \quad (1)$$

where J_w (L per (m^2 per h per bar)) is pure water flux; V (L) is the volume of filtrate; A (m^2) is the effective area of the membrane; t is the filtration time in (h).

The molecular mass cutoff is when a substance's rejection rate reaches 90%, determining the molecular weight cutoff of a membrane. For a composite nanofiltration membrane, the molecular mass cutoff is 1 g L^{-1} of PEG800. The TOC analyzer was used to determine the concentration of PEG800 in the stock solution and filtrate. The PEG800 rejection rate was then computed using the following eqn (2):

$$R = \frac{C_p - C_f}{C_p} \times 100\% \quad (2)$$

where R is the PEG800 retention rate, expressed as a percentage; C_p and C_f are the PEG800 concentrations in g L^{-1} of the filtrate and stock solution.

2.7 Membrane fouling analysis

Membrane fouling affects membrane-based separation performance in practical applications, negatively impacting permeability, use of energy, and durability. The membrane fouling was caused by RB5 dye adsorption and electrostatic attraction to the CPVC composite LNF membrane surface during the filtration of simulated RB5 dye wastewater. Higher membrane surface roughness led to increased RB5 dye adsorption and more severe fouling, resulting in higher filtration resistance (R_r + R_{ir}), where R_r and R_{ir} represent reversible and irreversible filtration resistance, respectively. If the membrane surface charge differs from the dye charge, electrostatic attraction increases fouling and resistance. RB5 dye carries a negative charge, so a positively charged membrane surface attracts it, increasing resistance. According to Darcy's law, eqn (3) is derived:

$$J = \frac{\Delta P}{\mu(R_m + R_{ir} + R_r)} \quad (3)$$

Table 1 Addition of chemicals and reaction time

TA/GA : PEI	TA/GA (g L^{-1})	PEI (g L^{-1})	TMC (%)	Crosslinking time/min	Deposition time/h
1 : 3	0.02	0.3	0.2	5 min	1 h
1.5 : 4.5	0.03	0.45	0.2	5 min	1 h
2 : 6	0.04	0.6	0.2	5 min	1 h
2.5 : 7.5	0.05	0.75	0.2	5 min	1 h
3 : 9	0.06	0.9	0.2	5 min	1 h
3.5 : 10.5	0.07	1.05	0.2	5 min	1 h

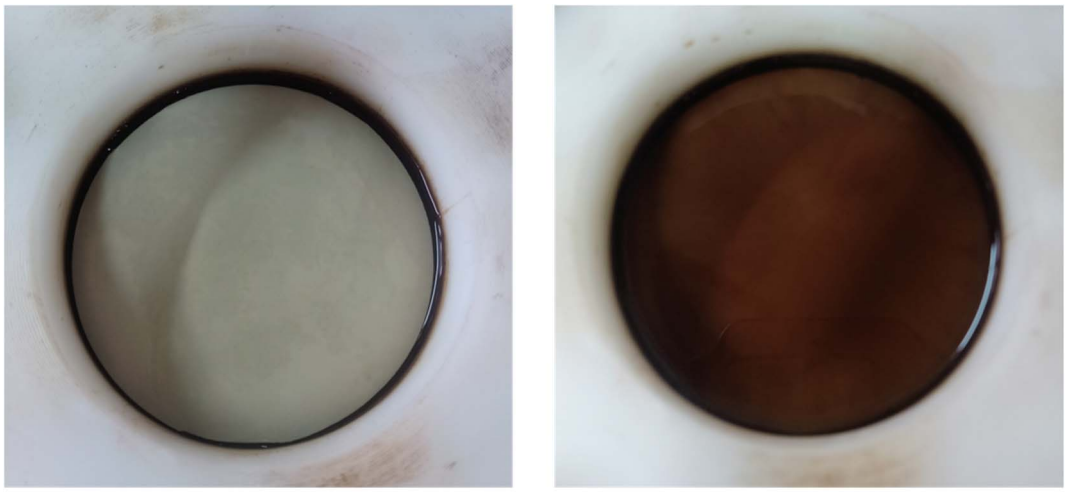

Fig. 1 Membrane variations during the experiment. (a) Before co-deposition. (b) After co-deposition for 1 h.

ΔP is the transmembrane pressure (MPa), and μ is the solution's dynamic viscosity (Pa s). R_m denotes the intrinsic membrane resistance (m^{-1}). R_{ir} is the irreversible contamination resistance (m^{-1}), whereas R_r is the reversible contamination resistance (m^{-1}).

Using eqn (1) and (3), R_m, R_{ir}, and R_r can be calculated as follows:

$$R_m = \frac{\Delta P}{\mu J_0} \quad (4)$$

$$R_{ir} + R_r = \frac{\Delta P}{\mu J_1} - \frac{\Delta P}{\mu J_0} \quad (5)$$

where J_0 and J_1 represent pure water flux and simulated dye wastewater flux in (L m^{-2} h^{-1}).

2.8 CPVC nanofiltration membrane simulation for RB5 and NaCl in dye wastewater

The methodologies used to determine the dye wastewater flux, dye, and salt rejection rates are identical to those used to determine the pure water flux and PEG800, respectively. Using a distilled water solution containing 0.1 g L^{-1} of RB5 and 0.05 g L^{-1} of NaCl, the simulated dye wastewater was treated. After 1 hour of pre-pressurization at 0.15 MPa for the CPVC composite loose nanofiltration membrane, the filtrate volume of the dye wastewater simulation was observed at 0.1 MPa and recorded hourly for six continuous hours. Eqn (1) was used to calculate the flux of dye wastewater. While eqn (2) was used to calculate the retention rate of salt and RB5 dye. A conductivity meter was used to determine the concentration of salt, and a UV-7504PC UV-visible spectrophotometer was used to measure the absorbance dye molecules at 593 nm of the RB5 in both the stock solution and filtrate. Filtration of dye wastewater for six hours can be seen in Fig. 2.

3. Results and discussion

3.1 Formation and chemical structures of selective layer of CPVC composite LNF membrane

The chemical structure of the selective layer the of CPVC composite loose nanofiltration membrane is reflected in the ATR-FTIR spectra presented in Fig. 3. Fig. 3(a) shows the stretching vibration of the C–Cl group is responsible for the characteristic peak of the CPVC base membrane at 645 cm^{-1}. In the composite loose nanofiltration membrane, the distinctive PEI peak at 2929 cm^{-1} disappears, which belongs to the amine peak. Additionally, it demonstrates that the composite CPVC loose nanofiltration membrane's surface forms polyamide (PA). It can be seen that the vibration peaks of the amine group and the phenolic hydroxyl group of TA/PEI disappear after 1700 cm^{-1}. A new peak belongs to the benzene ring C=C resonance vibration, the amide C=N overlap of tensile vibrations, and TMC and TA. The characteristic peak from 630 cm^{-1} to 3359 cm^{-1} belongs to the TA/PEI CPVC loose nanofiltration membrane.

Fig. 3(b) shows the chemical structure of the selective layer of the CPVC/GA/PEI composite loose nanofiltration membrane as reflected in the ATR-FTIR spectra. The CPVC base membrane's distinctive peak at 645 cm^{-1} is caused by the stretching vibration of the C–Cl group. The amine peak is located at 2929 cm^{-1}, where the characteristic PEI peak vanishes in the composite loose nanofiltration membrane. It can be seen that the vibration peaks of the amine group and the phenolic hydroxyl group of GA/PEI disappear after 1800 cm^{-1}. It is most likely because there are no substantial functional group vibrations in that range that account for the straight appearance of the curves for both TA and GA after 1800 cm^{-1} in the ATR-FTIR spectra, which results in a reasonably flat baseline for both materials. Less prominent or noticeable peaks could also arise from diminished sensitivity or instrumental limitations in this high wavenumber range.[51] Moreover, the concentration of TA and GA in

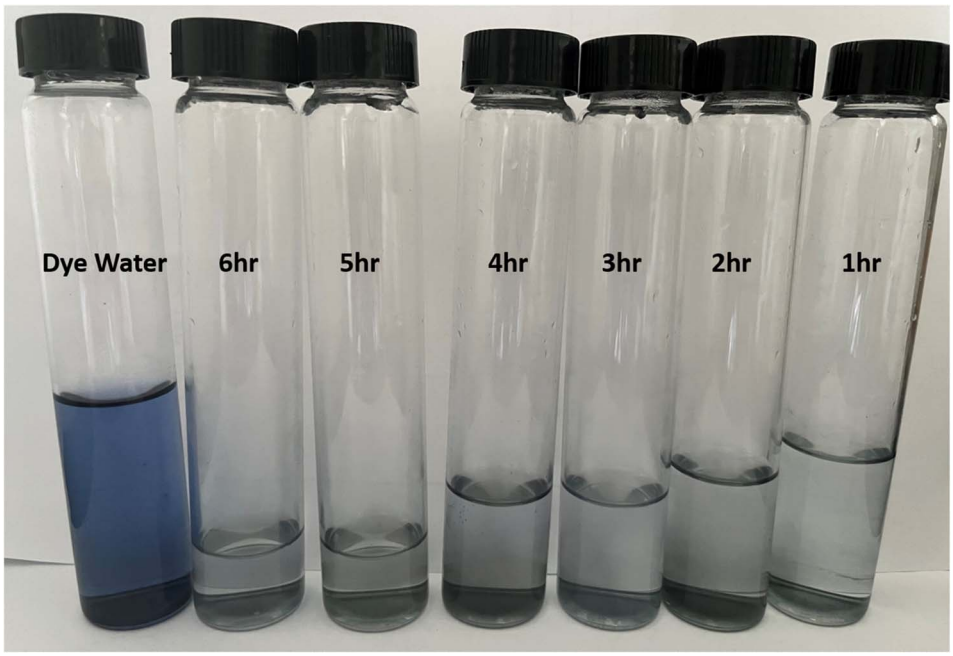

Fig. 2 Filtration of dye wastewater for six hours.

the composite membrane or the techniques used to prepare the sample may result in weaker signals that merge with the background noise to give the illusion of being straight.[52] This appearance may also be caused by overlapping peaks that the instrument is unable to adequately resolve. Comprehending these variables aids in elucidating the studied occurrences that were observed.

3.2 Morphology of CPVC composite LNF membrane

The cross-sectional microstructure and surface roughness of the CPVC composite LNM selective layer were characterized by FESEM and AFM images, as shown in Fig. 4 and 5. When the content of TA/PEI is higher, it leads to an increase in the surface roughness of the selection layer of the CPVC composite loose nanofiltration membrane. Along with this, the thickness of the selective layer also increases. As we can see in Fig. 4(a) and (b) at ratio 1 : 3, when the total content of TA is less than at ratios 2.5 : 7.5 and 3 : 9 in Fig. 4(d), (e) and (g), (h), the thickness of the selective layer is also increasing. This phenomenon arises due to tannic acid possessing a significantly higher hydroxyl content compared to gallic acid (GA). Moreover, TA, being a larger molecule with a higher molecular mass and hydroxyl content, tends to contribute to the formation of thicker selective layers in CPVC composite membranes. Consequently, during the reaction between tannic acid, polyethyleneimine (PEI), and trimesoyl chloride (TMC), more aggregates form on the membrane surface, consequently enhancing the membrane's roughness and causing a thickening of the selective layer.

When we come to the effects of GA/PEI on the surface roughness of the selective layer of the CPVC composite loose

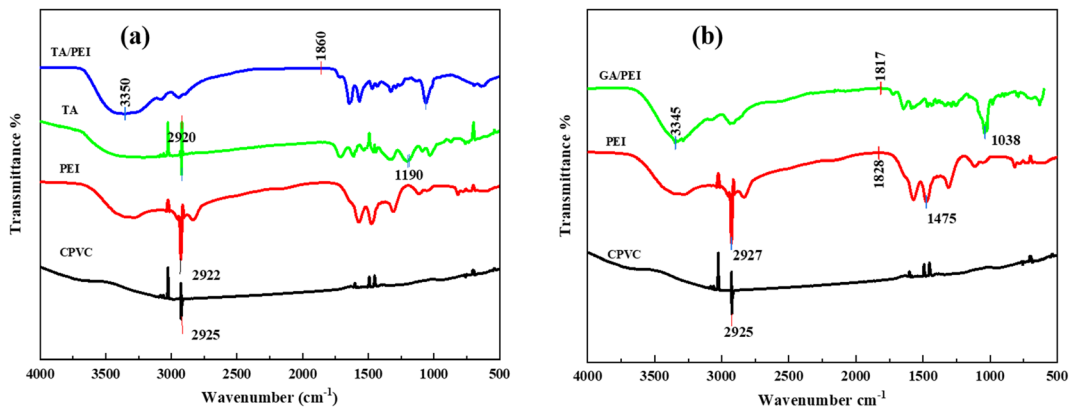

Fig. 3 (a) ATR-FTIR spectra of TA : PEI CPVC composite loose nanofiltration membrane; (b) ATR-FTIR spectra of GA : PEI CPVC composite loose nanofiltration membrane.

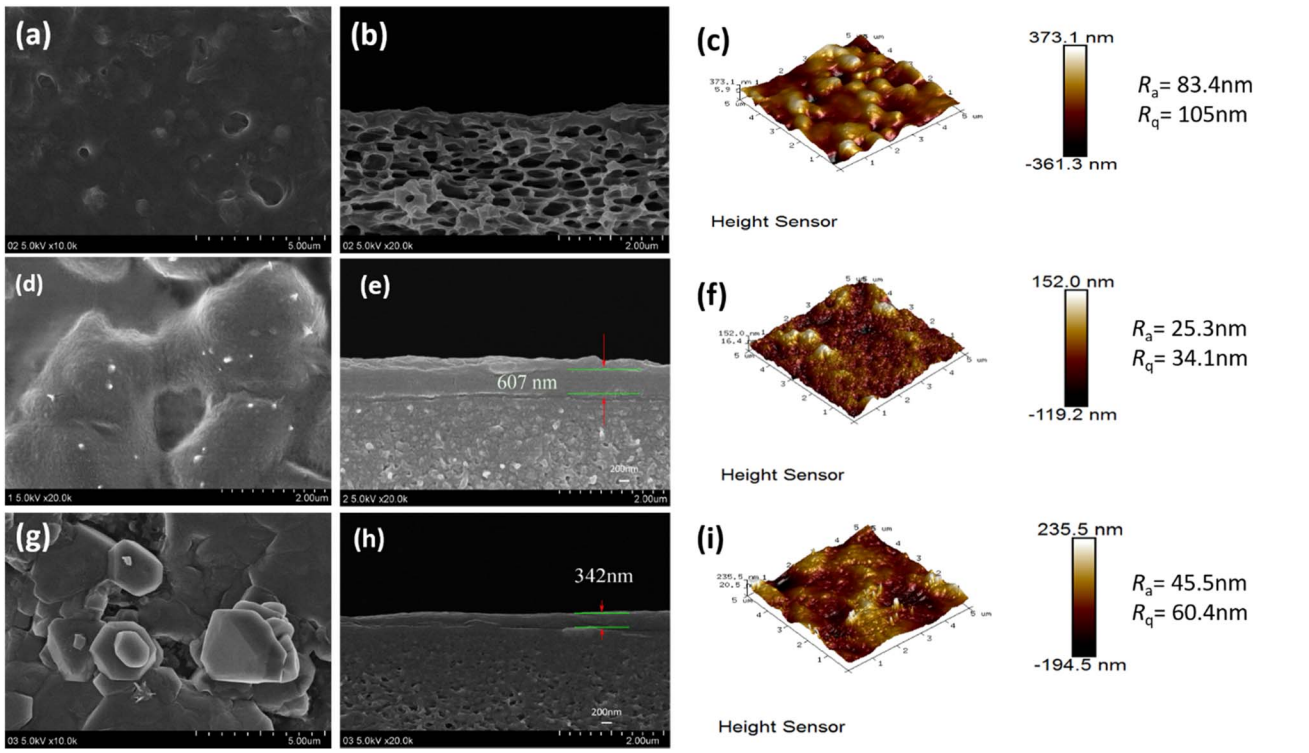

Fig. 4 SEM images of CPVC composite LNF membrane at different TA : PEI ratio: (a and b) 1 : 3, (d and e) 2.5 : 7.5, and (g and h) 3 : 9; and AFM images of LNF membrane at different ratio of TA : PEI; (c) 1 : 3, (f) 2.5 : 7.5, and (i) 3 : 9.

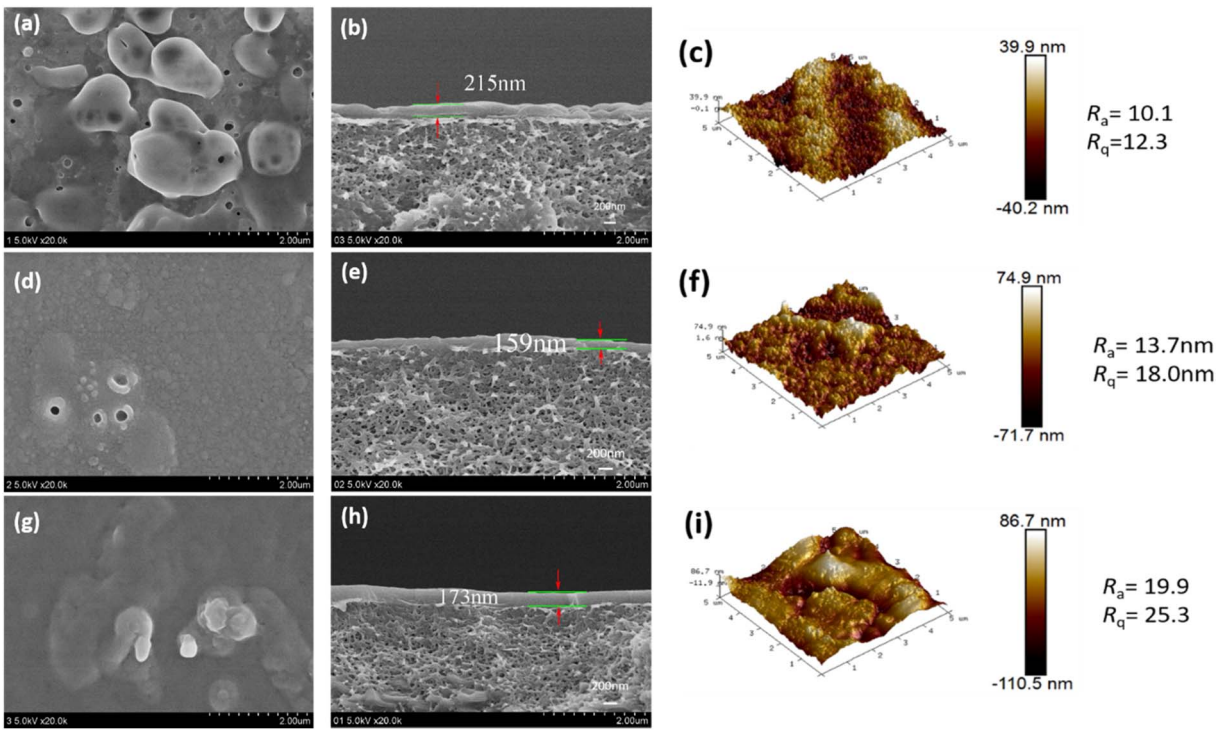

Fig. 5 SEM images of CPVC composite LNF membrane at different GA : PEI ratio: (a and b) 1 : 3, (d and e) 2.5 : 7.5, and (g and h) 3 : 9; and AFM images of LNF membrane at different ratio of GA : PEI; (c) 1 : 3, (f) 2.5 : 7.5, and (i) 3 : 9.

nanofiltration membrane. GA, on the other hand, may not contribute considerably to the creation of thicker selective layers due to its smaller molecular size, lower hydroxyl content, and molecular mass when compared to TA. The interaction of GA with PEI and TMC may not lead to as many aggregates on the membrane surface compared to TA, potentially resulting in a less pronounced increase in the membrane roughness and thickness of the selective layer. As we can see in Fig. 5(a) and (b), the thickness of the layer is less than in Fig. 5(d), (e) and (g), (h) because of the concentration of GA/PEI.

Size exclusion is one of the main methods of separation in nanofiltration membranes. Atomic force microscopy (AFM) and scanning electron microscopy (SEM) were used to examine the pore size distribution of the membranes. The pore diameters of the CPVC/TA/PEI and CPVC/GA/PEI membranes, as depicted in Fig. 4 and 5, are within the range that permits the passage of smaller ions, such as NaCl, while effectively allowing the rejection of dye molecules, such as reactive black 5.[53]

3.3 Hydrophilic characterization of CPVC composite LNF membrane

The surface hydrophilicity of the composite LNM is characterized by the water contact angle. The influence of water contact angle on the surface of the composite nanofiltration membrane is shown in Fig. 6. The hydrophilicity of the membrane surface decreased as the water contact angle increased with an increase in TA/PEI and the same with GA/PEI. Hence, the water contact angle on the surface of the membrane decreases; that is, the hydrophilicity of the surface of the membrane increases. The reason is that TA has a large number of carboxyl groups, which increases the hydrophilicity of the membrane surface.

3.4 CPVC composite loose nanofiltration membrane filtration performance test

3.4.1 Pure water flux and LNF membrane interception molecular weight analysis. The CPVC composite loose nanofiltration membrane, pure water flux, and PEG800 effect of the interception rates of TA/PEI and GA/PEI are shown in Fig. 7. The variation of PEG800 rejection and pure water flux with TA/PEI and GA/PEI for composite CPVC loose nanofiltration membranes is depicted in Fig. 7(a) and (b). Fig. 7(a) shows that when the total content of TA/PEI is 4 kg L^{-1}, the water flux is high, which is 7.5 L per m^2 per h per bar. However, as the total content of TA/PEI increases, the water flux starts decreasing, and the minimum flux is at the total content 10 kg L^{-1} which is 3.3 L per m^2 per h per bar, but as the total content of TA/PEI reaches 12 kg L^{-1} it starts increasing the flux again. However, the overall rejection rate of PEG800 is almost the same, at 98% for all concentration. Fig. 7(b) shows that the pure water flux of the CPVC composite LNF membrane for GA/PEI also shows the same trend as TA/PEI because when the total content of GA/PEI is 4 kg L^{-1}, the water flux is increasing. Hence, as the total content of GA/PEI increases, the water flux shows a decreasing trend. However, when the total content of GA/PEI reaches 12 kg L^{-1}, it starts increasing again. The highest flux is at the total content of 14 kg L^{-1}, which is 8.8 L per m^2 per h per bar and the minimum flux is at 8 kg L^{-1} and 10 kg L^{-1}. The overall PEG800 rejection rate for GA/PEI is also 97–98%. The reason behind the fluctuation of water flux is the polyester of the selective layer. Because when the polyester in the selective layer is too much, which makes it more porous. Hence, when the porosity is high, the flux will be high. If the porosity is low, then the flux is also low.

3.4.2 An empirical analysis of RB5 dye wastewater treatment. The effects of TA : PEI and GA : PEI on the filtration performance of CPVC composite loose nanofiltration membranes treating simulated RB5 dye wastewater are shown in Fig. 8(a) and (b). The coating parameters significantly affected the performance of the LNM. The filtration experiments used a 0.1 g L^{-1} CR aqueous solution. Previous research has explored the impact of average molecular weight and PEI percentage in coating solutions.[54] As shown in Fig. 8(a), the flux of RB5 is increasing when the total content of TA/PEI is 4 kg L^{-1}. As the total content of TA/PEI increases, the flux of the dye starts reducing, and the minimum flux of dye is at the total content of

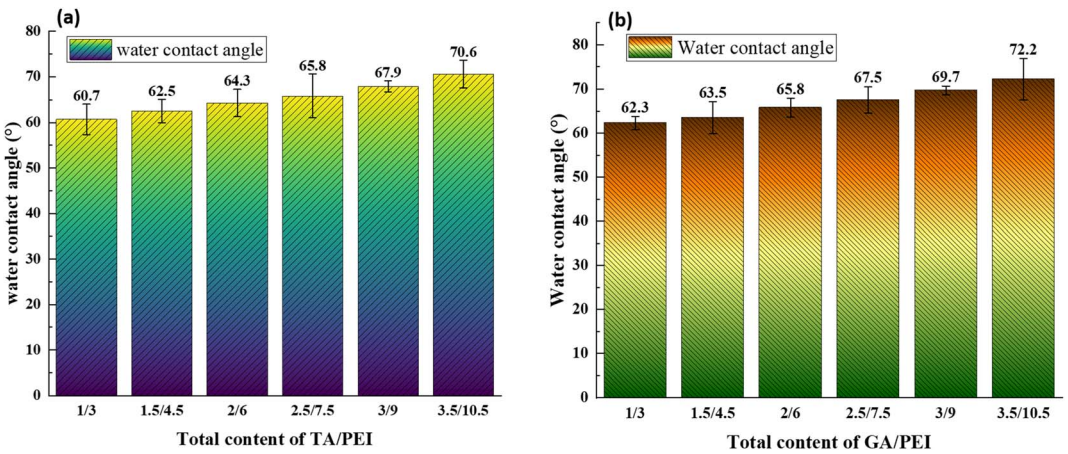

Fig. 6 Effect of water contact angle on CPVC composite LNF membrane; (a) effects of the total content of TA/PEI ratio on hydrophilicity of membrane surface; (b) effects of the total content of GA/PEI on hydrophilicity of membrane surface.

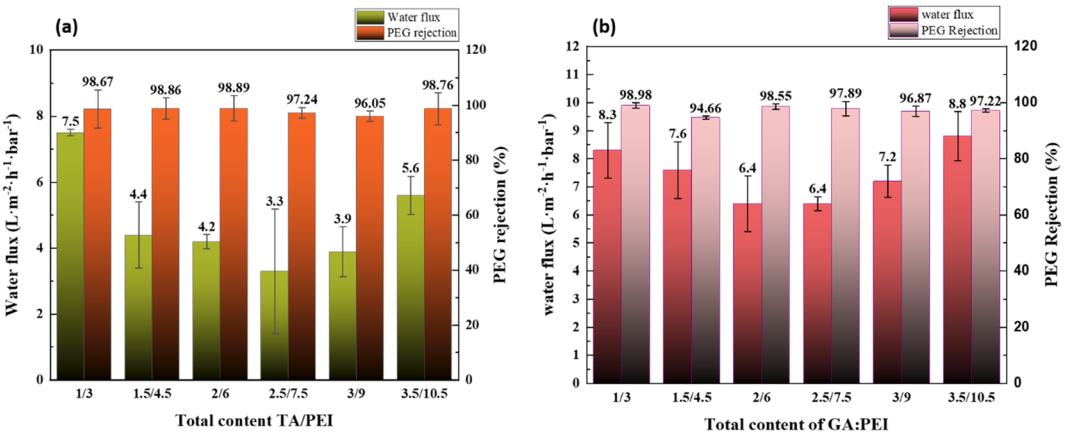

Fig. 7 (a) Effects of total content of TA : PEI ratio on the pure water flux and PEG800 retention rate on CPVC composite LNF membrane; (b) effects of total content of GA : PEI ratio on the pure water flux and PEG800 retention rate on CPVC composite LNF membrane.

10 kg L^{-1}. However, as the total content reaches 12 kg L^{-1}, it starts increasing again. Among these 6 concentrations, the highest flux rate is 6.4 L per (m^2 per h per bar) when the total content of TA/PEI is 4 kg L^{-1}, and it also has the highest rejection rate of 99.69%. The overall rejection rate of TA/PEI is 99%, and the NaCl retention rate gradually decreased from 4% to 3%. In Fig. 8(b), the flux of RB5 is increasing when the total content of GA/PEI is 4 kg L^{-1} and the flux is 5.5 L per (m^2 per h per bar). Afterwards, as the total content of GA/PEI increases the flux of dye wastewater starts reducing and reaches the minimum flux rate at a total content of 8 kg L^{-1}, which is 3.9 L per (m^2 per h per bar). However, when the total content reaches 12 kg L^{-1}, the flux of dye wastewater increases again and reaches the highest flux rate at 14 kg L^{-1}, which is 6.5 L per (m^2 per h per bar). The rejection rate of dye wastewater for GA/PEI is 97–99%. However, the flux of RB5 dye wastewater at all concentrations of GA : PEI is highest at the same concentrations as TA : PEI, but the rejection of TA : PEI is much better than that of GA : PEI. This is because of compared to gallic acid (GA), tannic acid has a substantially higher hydroxyl concentration. TA, being a larger molecule with a higher molecular mass and hydroxyl content, tends to contribute to the formation of thicker selective layers in CPVC composite membranes. In contrast, GA may not have a substantial effect on the development of larger selective layers because of its smaller molecular size, lower hydroxyl content, and lower molecular mass when compared to TA. The carbonyl groups in the PEI-TA layer can be attacked by nucleophiles and hydrolyzed using an acid or base catalyst. This could lead to increased permeability and a decrease in CR rejection by relaxing the skin layer.[55] From the results, the best ratio of TA : PEI is 1 : 3, whose flux as well as rejection rate are both high compared to other TA : PEI ratios. The optimal ratio from GA : PEI is 1/3 and 3.5/10.5, with 99.21% and 98.88% rejection rates and 5.5 and 6.5 L per (m^2 per h per bar) flux rates, respectively.

3.5 Stability of CPVC composite LNF membrane in treating simulated RB5 dye wastewater

3.5.1 Stability of CPVC composite LNF membrane in treating simulated RB5 dye wastewater for TA/PEI. The result of

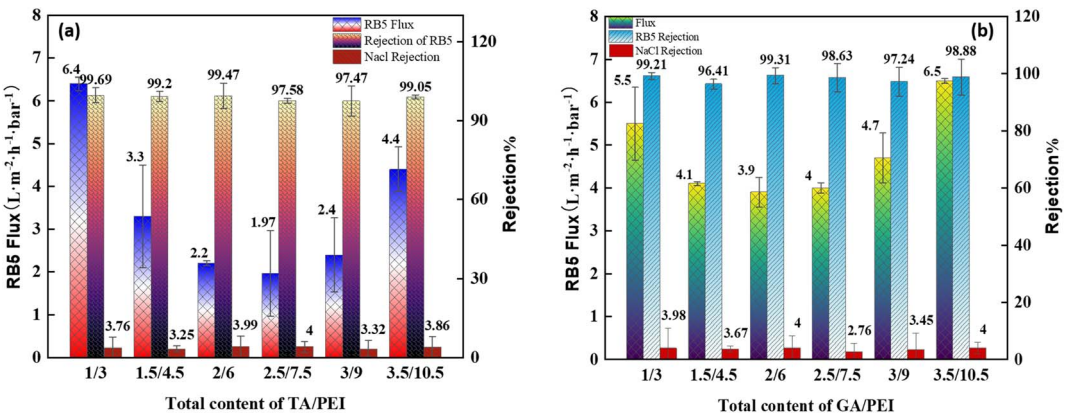

Fig. 8 (a) Effects of total content of TA : PEI ratio on the filtration performance of composite LNF membranes treating simulated RB5 dye wastewater; (b) effects of total content of GA : PEI ratio on the filtration performance of composite LNF membranes treating simulated RB5 dye wastewater.

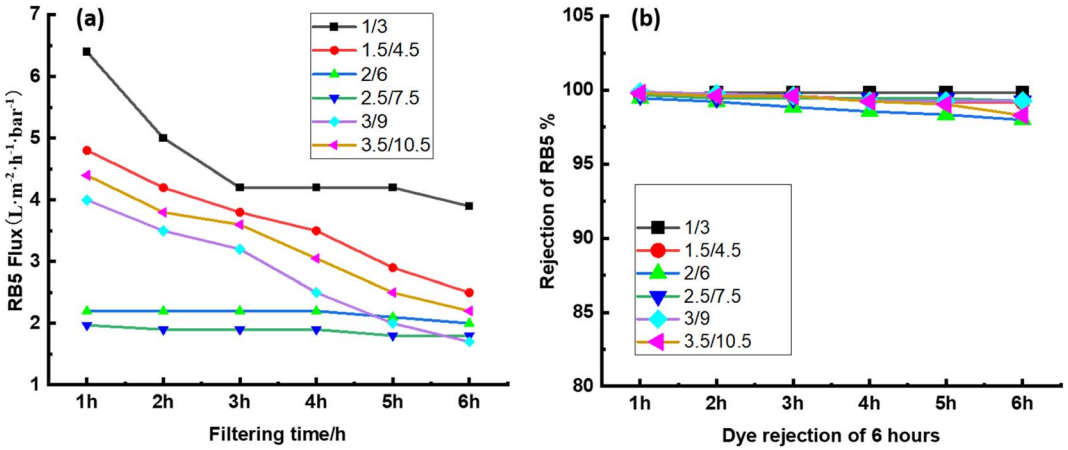

Fig. 9 Stability of CPVC composite LNF membrane in treating simulated RB5 dye wastewater for TA/PEI. (a) Filtration time per hour of RB5 wastewater for TA/PEI; (b) rejection rate of RB5 dye wastewater per hour for TA/PEI.

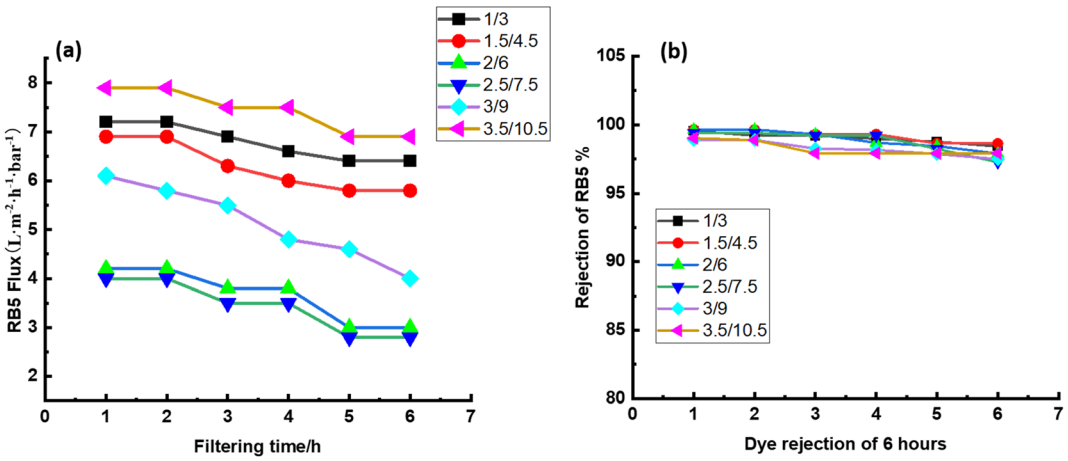

Fig. 10 Stability of CPVC composite LNF membrane in treating simulated RB5 dye wastewater for GA/PEI. (a) Filtration time per hour of RB5 wastewater for GA/PEI; (b) rejection rate of RB5 dye wastewater per hour for GA/PEI.

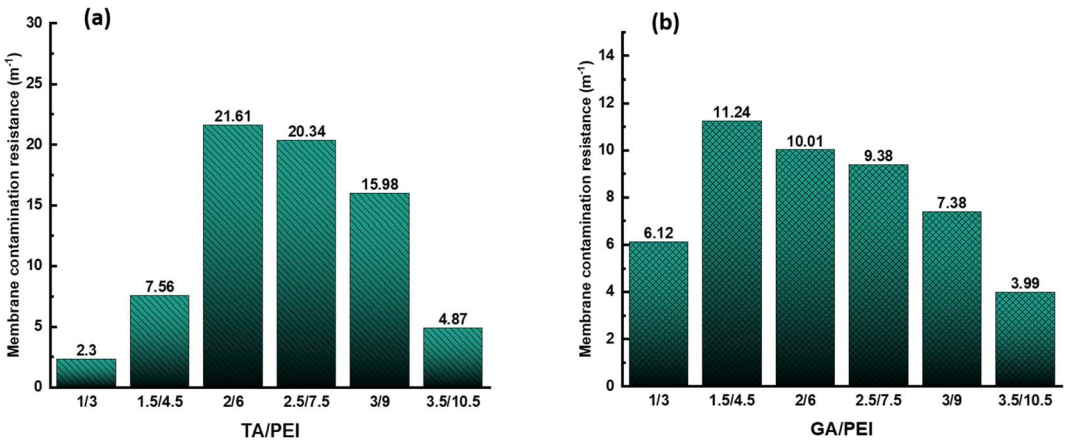

Fig. 11 (a) Irreversible and reversible fouling resistance of TA/PEI CPVC composite LNF membrane; (b) irreversible and reversible fouling resistance of GA/PEI CPVC composite LNF membrane.

Table 2 Comparison of loose NF performance between this work and other reported membranes

Support membrane	Permeability (L per m^2 per h per bar)	Dye	Rejection (%)	Salt rejection (%)	Ref.
GA/PEI/PAN	25.5	Congo red	97.1	5 NaCl	57
Sulfonated polyethylenimine (SPEI)-trimesoylchloride (TMC)/PSF	26.0	Congo red	98	3.2 = NaCl	58
Nano-TiO_2/PVA NF	5.4	Congo red	94	15 = Na_2SO_4	59
PVDF β-cyclodextrin	—	Brilliant green : congo red	97.4 96.4	NaCl = 15	60
PSF TMC/PIP, TA	—	Congo red : rose bengal	99.4 99.19	NaCl = 2.25	61
TMC/PEI, HACC, TiO_2	9.1	Reactive black 5	93.5	NaCl = 1.2	62
CPVC/TA/PEI	6.4	Reactive black 5	99.69	NaCl = 3–4	This work
CPVC/GA/PEI	6.5	Reactive black 5	99.31	NaCl = 3–4	This work

the operation stability of CPVC composite LNF membrane in treating simulated RB5 dye wastewater for TA/PEI is shown in Fig. 9. From Fig. 9(a), it can be seen that the RB5 dye wastewater flux decreasing with the time. However, intriguingly, in certain ratios, there appears to be a stabilization of flux as time progresses. Meanwhile from Fig. 9(b) it can be seen that the rejection of RB5 dye wastewater is constant for some ratios and it is decreasing for some ratios over the time.

3.5.2 Stability of CPVC composite LNF membrane in treating simulated RB5 dye wastewater for GA/PEI. The result of the operation stability of the CPVC composite LNF membrane in treating simulated RB5 dye wastewater for GA/PEI is shown in Fig. 10. We can see from Fig. 10(a) that the flux of RB5 dye wastewater is decreasing after 1 hour for all the ratios. The maximum flux is greater than 7 L per (m^2 per h per bar). However, from Fig. 10(b), we can see that the rejection of RB5 dye wastewater decreased after 1 hour for all the ratios. The maximum rejection rate is more than 99%.

3.6 Membrane fouling analysis

Fig. 11(a) and (b) demonstrate the fluctuation of the sum of irreversible (R_{ir}) and reversible (R_r) fouling resistance with TA/PEI and GA/PEI, respectively during the simulation of RB5 dye wastewater treatment by CPVC composite LNF membrane.

Fig. 11(a) shows that when the total content of TA/PEI increases, the value of $R_{ir} + R_r$ first increases and got the highest value at ratio 2/6; after that, the value of $R_{ir} + R_r$ starts decreasing. The rise in $R_{ir} + R_r$ with an increase in TA/PEI content could be attributed to improved interaction or crosslinking between the TA/PEI molecules, resulting in greater resistance. However, excess TA/PEI may cause aggregation of the membrane selective layer, lowering the efficiency of the interactions and resulting in a decrease in $R_{ir} + R_r$. While, as we can see in Fig. 11(b), the situation is the same. When the total content of GA/PEI increases, the value of $R_{ir} + R_r$ is also increasing initially, with the highest value at 1.5/4.5. Afterwards, the value of $R_{ir} + R_r$ start decreasing again. Hence, the initial increase followed by a decrease in $R_{ir} + R_r$ with increasing TA/PEI and GA/PEI content can be attributed to a balance between increased molecular interactions at lower ratios and the adverse effects of aggregation at higher ratios within the crosslinked network.

Long-term filtering tests were used to assess the membrane fouling resistance. The results demonstrate that the CPVC/GA/PEI and CPVC/TA/PEI membranes have a notable resistance to dye molecule fouling. Because hydrophilic surfaces are less likely to experience organic fouling, the hydrophilicity of the membranes—as demonstrated by measurements of the water contact angle (65°)—also helps to minimize fouling.[56]

A comparative analysis of the current CPVC composite LNF membrane's overall performance with that of other membranes that have been reported was carried out in light of the membrane's exceptional performance, and the results are presented in Table 2. Our CPVC composite membrane outperforms the majority of the other membranes listed, with a high dye rejection rate of 99.69%. Although competitive, the water flux is a little less than some others. Hence, we will continue to work on how to modify the permeability and hydrophilicity of membranes in our future work. This comparison places our work in the larger perspective of recent developments in membrane technology while also highlighting the efficacy of our membranes.

4. Conclusion

In this work, a CPVC composite loose nanofiltration membrane incorporated with plant polyphenols like TA and GA with PEI was successfully synthesized by interfacial polymerization with TMC and incorporated into the membrane surface with efficient dye/salt separation performance and high permeability was prepared. The result shows that the CPVC composite loose nanofiltration membrane's pure water flux fluctuates with increasing TA : PEI and GA : PEI concentrations, while the rejection rate of PEG800 remains consistent across all ratios. The flux and rejection rate of RB5 dye wastewater fluctuate with the changes in TA : PEI and GA : PEI concentrations. The optimal TA : PEI ratios reached a good pure water permeability up to 6.4 L per (m^2 per h per bar) with a high rejection rate of 99.69% to dye, and GA : PEI reached a good water permeability at 5.5 and 6.5 L per (m^2 per h per bar) with rejection rates of 99.31% and 99.21%, respectively, and the NaCl retention rate

gradually decreased from 4% to 3%. In order to assess the loose nanofiltration application and fractionate dye and salts from textile wastewater, our CPVC/TA/GA/PEI composite loose nanofiltration membrane performed as a competitive choice.

Data availability

The datasets created and/or analysed during the current investigation are accessible from the corresponding author upon reasonable request. The article and its accompanying materials provide all relevant data to support the study's findings. In addition, upon reasonable request, the corresponding author will provide any tools or code used for data analysis in this study.

Conflicts of interest

The authors declare no conflict of interest.

References

1 M. Kummu, J. H. Guillaume, H. de Moel, S. Eisner, M. Flörke, M. Porkka, S. Siebert, T. I. Veldkamp and P. Ward, *Sci. Rep.*, 2016, **6**, 38495.
2 C. N. Murphy, *The United Nations Development Programme: A Better Way?*, Cambridge University Press, 2006.
3 M. Bilal, M. Asgher, R. Parra-Saldivar, H. Hu, W. Wang, X. Zhang and H. M. N. Iqbal, *Sci. Total Environ.*, 2017, **576**, 646–659.
4 J. Lin, W. Ye, M.-C. Baltaru, Y. P. Tang, N. J. Bernstein, P. Gao, S. Balta, M. Vlad, A. Volodin, A. Sotto, P. Luis, A. L. Zydney and B. Van der Bruggen, *J. Membr. Sci.*, 2016, **514**, 217–228.
5 S. Ali, A. Khatri, U. Baig, A. Javeed and N. Ali Rind, *Color. Technol.*, 2020, **136**, 427–434.
6 C.-Z. Liang, S.-P. Sun, F.-Y. Li, Y.-K. Ong and T.-S. Chung, *J. Membr. Sci.*, 2014, **469**, 306–315.
7 J. Lin, W. Ye, H. Zeng, H. Yang, J. Shen, S. Darvishmanesh, P. Luis, A. Sotto and B. Van der Bruggen, *J. Membr. Sci.*, 2015, **477**, 183–193.
8 H. B. Park, J. Kamcev, L. M. Robeson, M. Elimelech and B. D. Freeman, *Science*, 2017, **356**, eaab0530.
9 J. H. Jhaveri and Z. V. P. Murthy, *Desalination*, 2016, **379**, 137–154.
10 P. Moradihamedani, *Polym. Bull.*, 2022, **79**, 2603–2631.
11 S. P. Bera, M. Godhaniya and C. Kothari, *J. Basic Microbiol.*, 2022, **62**, 245–259.
12 A. M. Nasir, M. R. Adam, S. N. E. A. M. Kamal, J. Jaafar, M. H. D. Othman, A. F. Ismail, F. Aziz, N. Yusof, M. R. Bilad and R. Mohamud, *Sep. Purif. Technol.*, 2022, **286**, 120454.
13 A. W. Mohammad, Y. Teow, W. Ang, Y. Chung, D. Oatley-Radcliffe and N. Hilal, *Desalination*, 2015, **356**, 226–254.
14 C. Fersi, L. Gzara and M. Dhahbi, *Desalination*, 2005, **185**, 399–409.
15 J. Wang, J. Zhu, M. T. Tsehaye, J. Li, G. Dong, S. Yuan, X. Li, Y. Zhang, J. Liu and B. Van der Bruggen, *J. Mater. Chem. A*, 2017, **5**, 14847–14857.
16 L. Chen, J.-H. Moon, X. Ma, L. Zhang, Q. Chen, L. Chen, R. Peng, P. Si, J. Feng, Y. Li, J. Lou and L. Ci, *Carbon*, 2018, **130**, 487–494.
17 A. W. Mohammad, Y. H. Teow, W. L. Ang, Y. T. Chung, D. L. Oatley-Radcliffe and N. Hilal, *Desalination*, 2015, **356**, 226–254.
18 J. Lin, C. Y. Tang, W. Ye, S.-P. Sun, S. H. Hamdan, A. Volodin, C. V. Haesendonck, A. Sotto, P. Luis and B. Van der Bruggen, *J. Membr. Sci.*, 2015, **493**, 690–702.
19 N. Khatoon, N. Ali, H. Yang and W. Jun, *Desalin. Water Treat.*, 2024, **317**, 100092.
20 B. Van der Bruggen, E. Curcio and E. Drioli, *J. Environ. Manage.*, 2004, **73**, 267–274.
21 S. Liu, Z. Wang and P. Song, *ACS Sustainable Chem. Eng.*, 2018, **6**, 4253–4263.
22 Q. Li, Z. Liao, X. Fang, D. Wang, J. Xie, X. Sun, L. Wang and J. Li, *J. Membr. Sci.*, 2019, **584**, 324–332.
23 M. Mozafari, S. F. Seyedpour, S. K. Salestan, A. Rahimpour, A. A. Shamsabadi, M. D. Firouzjaei, M. R. Esfahani, A. Tiraferri, H. Mohsenian and M. Sangermano, *J. Membr. Sci.*, 2019, **588**, 117200.
24 J. Zhu, A. Uliana, J. Wang, S. Yuan, J. Li, M. Tian, K. Simoens, A. Volodin, J. Lin, K. Bernaerts, Y. Zhang and B. Van der Bruggen, *J. Mater. Chem. A*, 2016, **4**, 13211–13222.
25 J. Zhu, M. Tian, Y. Zhang, H. Zhang and J. Liu, *Chem. Eng. J.*, 2015, **265**, 184–193.
26 P. Li, Z. Wang, L. Yang, S. Zhao, P. Song and B. Khan, *J. Membr. Sci.*, 2018, **555**, 56–68.
27 J. Zhu, J. Wang, A. A. Uliana, M. Tian, Y. Zhang, Y. Zhang, A. Volodin, K. Simoens, S. Yuan, J. Li, J. Lin, K. Bernaerts and B. Van der Bruggen, *ACS Appl. Mater. Interfaces*, 2017, **9**, 28990–29001.
28 J. Wang, L. Wang, M. He, X. Wang, Y. Lv, D. Huang, J. Wang, R. Miao, L. Nie and J. Hao, *RSC Adv.*, 2022, **12**, 34245–34267.
29 R. Zhang, Y. Liu, M. He, M. Wu, Z. Jiao, Y. Su, Z. Jiang, P. Zhang and X. Cao, *J. Membr. Sci.*, 2018, **555**, 337–347.
30 H. Zhang, L. Bin, J. Pan, Y. Qi, J. Shen, C. Gao and B. Van der Bruggen, *J. Membr. Sci.*, 2017, **539**, 128–137.
31 M. Li, Y. Yao, W. Zhang, J. Zheng, X. Zhang and L. Wang, *Environ. Sci. Technol.*, 2017, **51**, 9252–9260.
32 W. J. Lau, S. Gray, T. Matsuura, D. Emadzadeh, J. Paul Chen and A. F. Ismail, *Water Res.*, 2015, **80**, 306–324.
33 H. Zhang, B. Li, J. Pan, Y. Qi, J. Shen, C. Gao and B. Van der Bruggen, *J. Membr. Sci.*, 2017, **539**, 128–137.
34 X. Wei, S. Wang, Y. Shi, H. Xiang and J. Chen, *Ind. Eng. Chem. Res.*, 2014, **53**, 14036–14045.
35 L. Pan, H. Wang, C. Wu, C. Liao and L. Li, *ACS Appl. Mater. Interfaces*, 2015, **7**, 16003–16010.
36 L. Pérez-Manríquez, P. Neelakanda and K.-V. Peinemann, *J. Membr. Sci.*, 2017, **541**, 137–142.
37 M.-B. Wu, X.-L. Fan, H.-C. Yang, J. Yang, M.-M. Zhu, K.-F. Ren, J. Ji and Z.-K. Xu, *J. Membr. Sci.*, 2019, **570–571**, 270–277.

38 X. Fang, J. Li, X. Li, S. Pan, X. Sun, J. Shen, W. Han, L. Wang and B. Van der Bruggen, *J. Colloid Interface Sci.*, 2017, **505**, 642–652.
39 Z. Yang, Z.-w. Zhou, H. Guo, Z. Yao, X.-h. Ma, X. Song, S.-P. Feng and C. Y. Tang, *Environ. Sci. Technol.*, 2018, **52**, 9341–9349.
40 X. Zhao, N. Jia, L. Cheng, L. Liu and C. Gao, *J. Membr. Sci.*, 2018, **563**, 435–446.
41 X. Fang, J. Li, B. Ren, Y. Huang, D. Wang, Z. Liao, Q. Li, L. Wang and D. D. Dionysiou, *J. Membr. Sci.*, 2019, **579**, 190–198.
42 Y. Zhang, Y. Su, J. Peng, X. Zhao, J. Liu, J. Zhao and Z. Jiang, *J. Membr. Sci.*, 2013, **429**, 235–242.
43 M.-Y. Lim, Y.-S. Choi, J. Kim, K. Kim, H. Shin, J.-J. Kim, D. M. Shin and J.-C. Lee, *J. Membr. Sci.*, 2017, **521**, 1–9.
44 M. Li, W. van Keulen, M. van de Ven, A. Molenaar and G. Tang, *Constr. Build. Mater.*, 2014, **59**, 62–71.
45 Y. Lv, H.-C. Yang, H.-Q. Liang, L.-S. Wan and Z.-K. Xu, *J. Membr. Sci.*, 2015, **476**, 50–58.
46 Z. Zhu, Y. Liu, H. Hou, W. Shi, F. Qu, F. Cui and W. Wang, *Environ. Sci. Technol.*, 2018, **52**, 3027–3036.
47 X. Q. Cheng, Z. X. Wang, J. Guo, J. Ma and L. Shao, *ACS Sustainable Chem. Eng.*, 2018, **6**, 1881–1890.
48 N. Zhang, X. Song, Y. Chen, B. Jiang, L. Zhang and H. Jiang, *Environ. Sci. Water Res. Technol.*, 2021, **7**, 956–968.
49 J. Y. Sum, A. L. Ahmad and B. S. Ooi, *J. Membr. Sci.*, 2014, **466**, 183–191.
50 S. Li, Z. Wang, C. Zhang, M. Wang, F. Yuan, J. Wang and S. Wang, *J. Membr. Sci.*, 2013, **436**, 121–131.
51 B. C. Smith, *Fundamentals of Fourier Transform Infrared Spectroscopy*, CRC press, 2011.
52 M. S. Robert, X. W. Francis, J. K. David, and B. L. David, *Spectrometric identification of organic compounds*, John Wiley & Sons, Inc., 7 edn, 2005, vol. 106.
53 M. Khraisheh, S. Elhenawy, F. AlMomani, M. Al-Ghouti, M. K. Hassan and B. H. Hameed, *Membranes*, 2021, **11**, 995.
54 Y. C. Xu, Z. X. Wang, X. Q. Cheng, Y. C. Xiao and L. Shao, *Chem. Eng. J.*, 2016, **303**, 555–564.
55 K. P. Lee, J. Zheng, G. Bargeman, A. J. B. Kemperman and N. E. Benes, *J. Membr. Sci.*, 2015, **478**, 75–84.
56 T. A. Geleta, I. V. Maggay, Y. Chang and A. Venault, *Membranes*, 2023, **13**(1), DOI: **10.3390/membranes13010058**.
57 S. Zhao and Z. Wang, *J. Membr. Sci.*, 2017, **524**, 214–224.
58 J. Ding, H. Wu and P. Wu, *Chem. Eng. J.*, 2020, **396**, 125199.
59 X. Li, Y. Chen, X. Hu, Y. Zhang and L. Hu, *J. Membr. Sci.*, 2014, **471**, 118–129.
60 J. Li, J.-L. Gong, G.-M. Zeng, B. Song, W.-C. Cao, S.-Y. Fang, S.-Q. Tang, Y. Guan, Z.-K. Tan, Z.-P. Chen, X.-Q. Mao and R.-L. Zhu, *Sep. Purif. Technol.*, 2021, **276**, 119352.
61 Q. Li, Z. Liao, X. Fang, J. Xie, L. Ni, D. Wang, J. Qi, X. Sun, L. Wang and J. Li, *Desalination*, 2020, **479**, 114343.
62 X. Bai, Y. Zhang, H. Wang, H. Zhang and J. Liu, *Desalination*, 2013, **313**, 57–65.